Electronic properties of GaAs, InAs and InP nanowires studied by terahertz spectroscopy

Hannah J Joyce[1], Callum J Docherty[1], Qiang Gao[2], H Hoe Tan[2], Chennupati Jagadish[2], James Lloyd-Hughes[1], Laura M Herz[1] and Michael B Johnston[1]

[1] Department of Physics, University of Oxford, Clarendon Laboratory, Oxford OX1 3PU, UK
[2] Department of Electronic Materials Engineering, Research School of Physics and Engineering, The Australian National University, Canberra, ACT 0200, Australia

E-mail: h.joyce1@physics.ox.ac.uk and m.johnston@physics.ox.ac.uk

Abstract

We have performed a comparative study of ultrafast charge carrier dynamics in a range of III–V nanowires using optical pump–terahertz probe spectroscopy. This versatile technique allows measurement of important parameters for device applications, including carrier lifetimes, surface recombination velocities, carrier mobilities and donor doping levels. GaAs, InAs and InP nanowires of varying diameters were measured. For all samples, the electronic response was dominated by a pronounced surface plasmon mode. Of the three nanowire materials, InAs nanowires exhibited the highest electron mobilities of 6000 cm^2 V^{-1} s^{-1}, which highlights their potential for high mobility applications, such as field effect transistors. InP nanowires exhibited the longest carrier lifetimes and the lowest surface recombination velocity of 170 cm s^{-1}. This very low surface recombination velocity makes InP nanowires suitable for applications where carrier lifetime is crucial, such as in photovoltaics. In contrast, the carrier lifetimes in GaAs nanowires were extremely short, of the order of picoseconds, due to the high surface recombination velocity, which was measured as 5.4×10^5 cm s^{-1}. These findings will assist in the choice of nanowires for different applications, and identify the challenges in producing nanowires suitable for future electronic and optoelectronic devices.

(Some figures may appear in colour only in the online journal)

1. Introduction

III–V semiconductor nanowires, such as GaAs, InAs and InP nanowires, show enormous promise as active components in solar cells [1], photodetectors [2], light-emitting diodes [3] and ultrahigh density transistors [4]. The future development of these nanowire-based devices requires a thorough understanding of charge carrier dynamics and transport in nanowires. Progress in understanding these properties has, however, been hampered because conventional techniques for measuring electrical transport require lithographically placed electrical contacts to individual nanowires, and the measurements are subject to artefacts arising from the

electrical contacts and the models used to extract transport parameters [5, 6]. Contact-free measurements of carrier dynamics have largely been limited to photoluminescence (PL) investigations at low temperatures [7, 8]. Noncontact measurements at room temperature are less frequently reported, one example being the recent transmission Raman spectroscopy measurements of hole mobility in p-type GaAs nanowires [9]. Room temperature measurements such as these are essential, because future nanowire-based devices will be operated at room temperature.

With these considerations in mind, one especially promising and versatile technique is optical pump–terahertz probe (OPTP) time domain spectroscopy [10, 11]. OPTP

spectroscopy is a noncontact room temperature technique with the capability to measure both carrier mobility and lifetime on timescales from under 1 ps to over 1 ns, and is therefore particularly well suited to studies of carrier transport in nanowires [12].

In this contribution we examine carrier lifetimes and mobilities in GaAs, InAs and InP nanowires using OPTP spectroscopy. The comparison of the three materials allows us to identify which nanowire types are suitable for different applications. These measurements also allow us to compare nanowire properties to those of bulk materials, and to identify future challenges in improving nanowire properties by tailoring growth techniques or by using surface passivation. We found that the carrier lifetimes in GaAs nanowires are extremely sensitive to nanowire diameter, and attribute the short 1–5 ps carrier lifetimes to the very high surface recombination velocity at GaAs surfaces. In marked contrast, carrier lifetimes in InP nanowires were consistently greater than 1 ns regardless of nanowire diameter, owing to the very low surface recombination velocity of InP surfaces. From photoconductivity spectra we measured the electron mobilities of GaAs, InAs and InP nanowires. We found that InAs nanowires exhibited the highest mobilities, of 6000 cm^2 V^{-1} s^{-1}, which is amongst the highest room temperature mobilities reported for nanowires [13]. This suggests the potential of InAs nanowires for high mobility applications. Additionally, we present a method which allows us to use OPTP measurements to measure the levels of unintentional doping present in the nanowires.

2. Experimental method

2.1. Nanowire sample preparation

Nanowires were grown by metal–organic chemical vapour deposition (MOCVD) using Au nanoparticles to direct nanowire growth. GaAs, InAs and InP nanowires were grown on GaAs(111)B, InAs(111)B and InP(111)B substrates, respectively. The substrates were treated with poly-*L*-lysine and separate pieces were treated with 20, 30, 50 or 80 nm diameter colloidal Au nanoparticles. These four different nanoparticle sizes were used so that different diameter nanowires could be grown, as the Au nanoparticle diameter is a principal determinant of nanowire diameter. GaAs nanowires were grown with trimethylgallium (TMG) and arsine (AsH$_3$) precursors via a two-temperature growth procedure [14] with growth at 375 °C and a V/III ratio of 46. InAs nanowires were grown using trimethylindium (TMI) and AsH$_3$ at a temperature of 400 °C and V/III ratio of 46. InP nanowires were grown using TMI and phosphine (PH$_3$) precursors at 420 °C and V/III ratio of 700. The growth conditions for GaAs and InAs nanowires were chosen to achieve zinc-blende (ZB) crystal structure with minimal twin defects [15]. The InP nanowires featured predominantly wurtzite (WZ) crystal structure with thin ZB sections and stacking faults [16].

The nanowires were then transferred to *z*-cut quartz by rubbing the as-grown substrates against the quartz substrates.
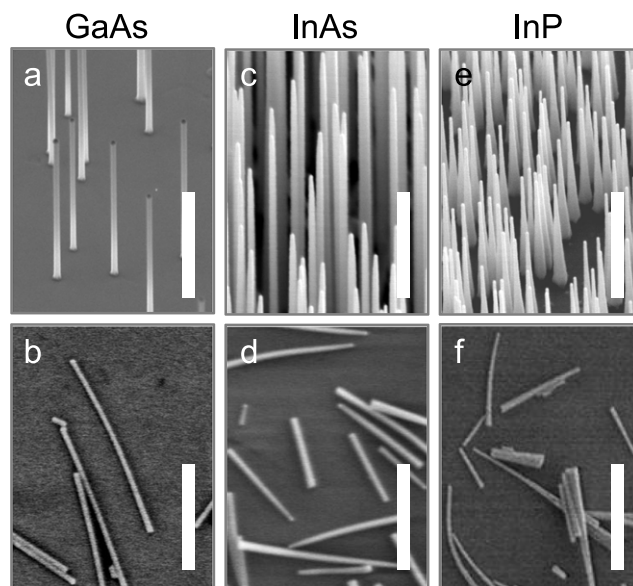

Figure 1. SEM images of ((a), (b)) GaAs nanowires of 50 nm average diameter, ((c), (d)) InAs nanowires of 45 nm average diameter and ((e), (f)) InP nanowires of 50 nm average diameter. Images (a), (c) and (e) show nanowires as-grown on original (111)B substrates at a tilt of 40°. Images (b), (d) and (f) show nanowires transferred to quartz substrates for OPTP measurements. Scale bars are 1 μm.

The quartz substrates do not exhibit any photoconductivity response, so are appropriate host substrates for OPTP measurements of nanowires. Figure 1 illustrates typical scanning electron microscope (SEM) images of as-grown nanowires and of nanowires on quartz. Each quartz substrate hosted randomly oriented nanowires of a particular average diameter. This average diameter was measured by SEM according to a procedure outlined previously [16]. The nanowire diameters were dictated by the diameter of the original Au nanoparticles and the amount of radial growth on the nanowire sidewalls. GaAs nanowires exhibited minimal radial growth and the 30, 50 and 80 nm diameter nanoparticles respectively gave rise to 30, 50 and 80 nm diameter GaAs nanowires. InAs nanowires exhibited more radial growth so that the 20, 30, 50 and 80 nm diameter nanoparticles resulted in wider average nanowire diameters of 27, 45, 95 and 195 nm, respectively. InP nanowires exhibited significant radial growth, giving average nanowire diameters of 50, 85, 135 and 160 nm. Hereafter, nanowires will be referred to by their average diameters on the quartz substrates.

2.2. Optical pump–terahertz probe spectroscopy

We performed OPTP measurements using a terahertz spectrometer described previously [16]. Briefly, the nanowires were photoexcited with an optical pump pulse centred at 800 nm with a duration of 35 fs. Photoexcitation fluences between 1 and 100 μJ cm^{-2} were used. Photoexcitation of the sample induced a change ΔE in the transmission of the terahertz probe pulse. The spectrometer measured the transmitted terahertz electric field: E without photoexcitation, and $E - \Delta E$ with photoexcitation.
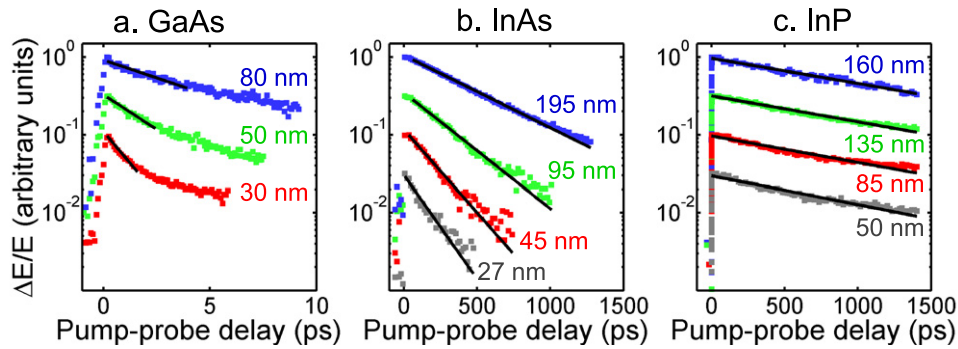
Figure 2. Pump-induced change in terahertz electric field ($\Delta E/E$) at different pump–probe delays. (a) $\Delta E/E$ decays for 30, 50, and 80 nm diameter GaAs nanowires, fitted with carrier lifetimes of $\tau = 1.3$, 2.4 and 4.7 ps, respectively. (b) $\Delta E/E$ decays for 27, 45, 95 and 195 nm diameter InAs nanowires, fitted with carrier lifetimes of $\tau = 200$, 290, 470 and 660 ps, respectively. (c) $\Delta E/E$ decays for 50, 85, 135 and 160 nm diameter InP nanowires, fitted with carrier lifetimes of $\tau = 1.18$, 1.27, 1.30 and 1.34 ns, respectively. These are scaled for clarity. The photoexcitation pump fluence was 10 μJ cm^{-2}. Straight lines are monoexponential fits to the decays at early times after photoexcitation. Data in (c) are reproduced with permission from [16]. (Copyright 2012 American Chemical Society.)

The differential transmission ΔE of the terahertz pulse can be directly converted to the photoinduced conductivity, $\Delta\sigma$, of the nanowires as outlined previously [16]. In this manner, the photoconductivity spectra of section 3.2 were obtained. The pump–probe decay curves of section 3.1 were produced by measuring ΔE at the peak of the terahertz pulse, as a function of delay after the photoexcitation pulse. We performed all analyses with the approximation that the measured photoconductivity arises from photoexcited electrons only, because in III–V semiconductors the hole effective mass is significantly larger than the electron effective mass.

3. Results and discussion

3.1. Photoconductivity decay

Our first comparison between nanowire material systems concerns carrier lifetime and the effect of nanowire surfaces. Due to the very high surface area-to-volume ratios intrinsic to nanowires, surface states can have a marked influence on the electronic properties of the nanowires. Significantly, surface states act as nonradiative recombination centres which can substantially reduce the carrier lifetime in the semiconductor.

To determine the role of surfaces states in each nanowire material system, we have measured photoconductivity lifetimes for several samples of different diameters. The smaller the nanowire diameter, the higher the surface area-to-volume ratio. Decays of $\Delta E/E$ are presented in figure 2, along with monoexponential fits to the decays. Monoexponential functions provide suitable fits to the decay traces for both InAs and InP nanowires. The decay traces for GaAs nanowires deviate from monoexponential behaviour due to saturable carrier trapping at nanowire surfaces [17]. Specifically, as photoexcited carriers are rapidly trapped at surface states, the surface traps become filled, so that the rate of carrier trapping slows with time after photoexcitation [17]. To obtain an accurate view of surface recombination when the surface traps are originally unoccupied, we have fitted the GaAs nanowire data at early times after photoexcitation.

From figure 2 it is clear that the photoconductivity of GaAs nanowires decays rapidly on picosecond timescales, and that this lifetime is strongly dependent on nanowire diameter. Smaller nanowire diameters feature the fastest decays. The carrier lifetime in InAs nanowires is longer, but is similarly dependent on nanowire diameter. InP nanowires, in contrast, feature long carrier lifetimes of over 1 ns with minimal dependence on nanowire diameter. The observations are correlated with the surface recombination velocity of these materials, which is known to be highest for GaAs and lowest for InP [18]. To further examine this, we calculate the surface recombination velocity for each material as follows.

The effective recombination time in nanowires is closely approximated by the function [16, 19]:

$$\frac{1}{\tau} = \frac{1}{\tau_{\text{volume}}} + \frac{4S}{d} \tag{1}$$

where d is the nanowire diameter, S is the surface recombination velocity and τ_{volume} is the time constant for recombination at volume defects. By fitting equation (1) to the experimental τ values we extract surface recombination velocities of 5.4×10^5, 3.0×10^3 and 170 cm s^{-1} for GaAs, InAs and InP surfaces, respectively. These values are consistent with results obtained for bulk GaAs [20, 21], InAs [22] and InP [23–25]. The very high surface recombination velocity of GaAs nanowires points to the importance of surface passivation. Surface passivation has been shown to increase the carrier lifetime in GaAs nanowires [17, 26] and improve band-edge PL emission from InAs nanowires [27]. In contrast, the remarkably low surface recombination velocity of InP nanowires makes them promising for many electronic applications, such as photovoltaics, which require long carrier lifetimes.

3.2. Photoconductivity spectra

The next comparison of GaAs, InAs and InP nanowires uses photoconductivity spectra to assess carrier scattering, carrier mobilities and doping levels. We measured photoconductivity spectra at a number of different fluences and times after
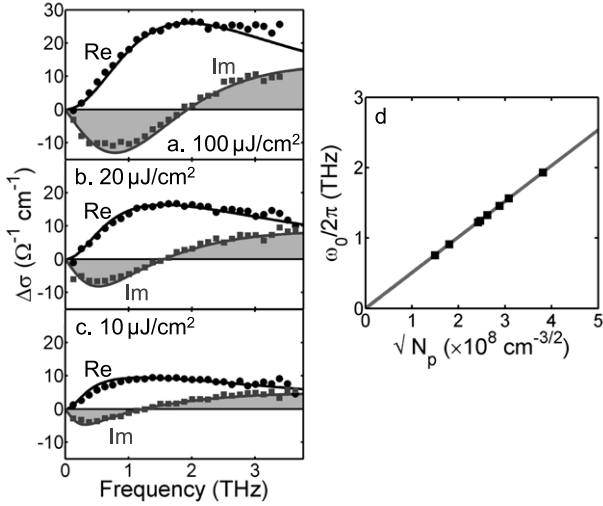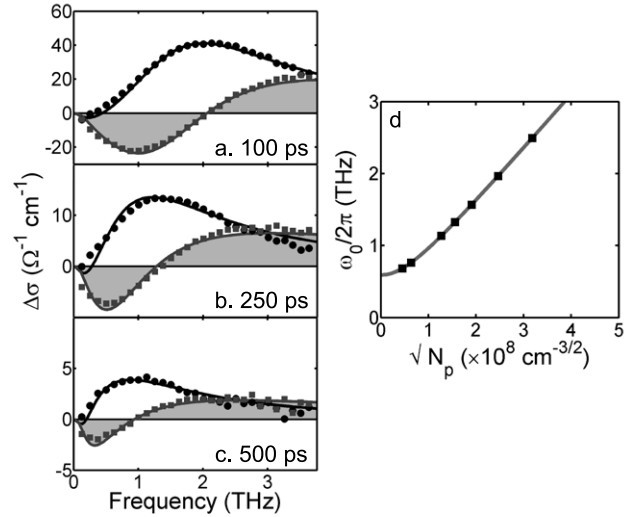
Figure 3. Fluence dependence of terahertz conductivity of 50 nm diameter GaAs nanowires. All spectra were taken at 2 ps after photoexcitation. ((a)–(c)) Photoinduced conductivity with photoexcitation fluences of (a) 100 (b) 20 and (c) 10 μJ cm^{-2}. The symbols are the measured data and the lines are the fitted plasmon responses. The real (black circles and lines) and imaginary (grey squares and lines) components of the conductivity are plotted. (d) Surface plasmon frequencies ω_0 extracted from the complete set of measured spectra.

Figure 4. Time-resolved conductivity of photoexcited carriers in 45 nm diameter InAs nanowires at times (a) 100 ps, (b) 250 ps and (c) 500 ps after the pump excitation pulse. The incident pump pulse fluence was 10 μJ cm^{-2}. The symbols are the measured data and the lines are the fitted plasmon responses. The real (black circles and lines) and imaginary (grey squares and lines) components of the conductivity are plotted. (d) Surface plasmon frequencies ω_0 extracted from the complete set of measured spectra.
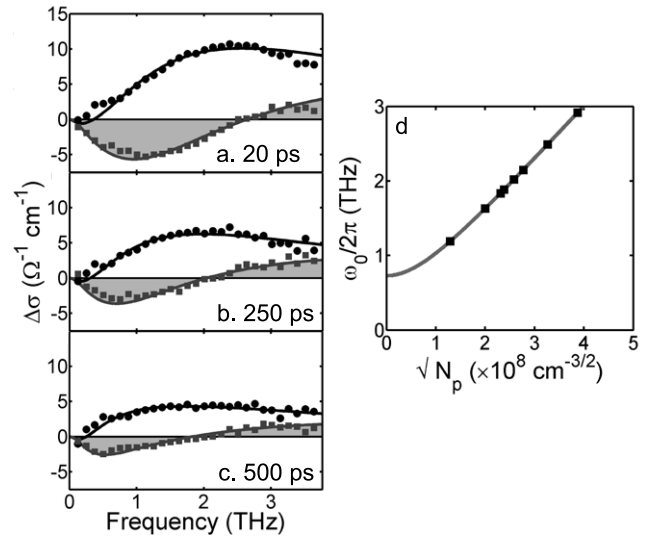
photoexcitation. Figure 3 illustrates typical photoconductivity spectra obtained for GaAs nanowires at different photoexcitation fluences. Figures 4 and 5 show typical photoconductivity spectra obtained for InAs and InP nanowires, respectively, at different times after photoexcitation. So that the results are comparable, we measured nanowires of similar average diameters: 50 nm for GaAs nanowires, 45 nm for InAs nanowires and 50 nm for InP nanowires. These samples correspond to the SEM images of figure 1.

All the spectra featured a pronounced Lorentzian response. As illustrated in figure 3, the resonance shifts to higher frequencies with increasing photoexcitation fluence. The resonance shifts to lower frequencies with time after photoexcitation, as evident in figures 4 and 5. In this manner, the resonant frequency increases with increasing carrier density, which is characteristic of localized surface plasmon (LSP) modes [28]. This type of response is well characterized for metallic nanostructures, which exhibit LSP modes in the ultraviolet, visible and near infrared ranges. In semiconductor nanostructures, with lower carrier densities than their metallic counterparts, LSP resonances fall in the terahertz range. Terahertz LSP modes have been observed in a variety of semiconductor nanostructures and microstructures, such as Si microstructures [28, 29], and GaAs [30], GaN [31], InAs [32], InP [16] and Ge nanowires [33]. We therefore attribute the response to a surface plasmon mode. The complex photoconductivity of a free electron plasma with a surface plasmon resonance is given by

$$\Delta\sigma = \frac{iN_p e^2 \omega}{m_e^*(\omega^2 - \omega_{0,N_p}^2 + i\omega\gamma)}, \quad (2)$$

Figure 5. Time-resolved conductivity of photoexcited carriers in 50 nm diameter InP nanowires at times (a) 20 ps, (b) 250 ps and (c) 500 ps after the pump excitation pulse. The incident pump pulse fluence was 10 μJ cm^{-2}. The symbols are the measured data and the lines are the fitted plasmon responses. The real (black circles and lines) and imaginary (grey squares and lines) components of the conductivity are plotted. (d) Surface plasmon frequencies ω_0 extracted from the complete set of measured spectra. Data in ((a)–(c)) are reproduced with permission from [16]. (Copyright 2012 American Chemical Society.)

where N_p is the photoexcited carrier density, e is the electronic charge, m_e^* is the electron effective mass, ω_0 is the surface plasmon resonance and γ is the momentum scattering rate. The surface plasmon frequency is a function of N_p, and is

Table 1. Parameters extracted for the nanowire samples, including surface recombination velocity (S), ionized donor density (N_d), electron scattering rate (γ) and electron mobility (μ). The quantities in brackets indicate the range of parameters giving adequate fits. The uncertainty in S is less than 10%. Typical electron mobilities (μ_{bulk}) for bulk semiconductors are also given [40, 44, 45].

Nanowires	S (cm s^{-1})	N_d ($\times 10^{15}$ cm^{-3})	γ ($\times 10^{13}$ s^{-1})	μ (cm^2 V^{-1} s^{-1})	μ_{bulk} (cm^2 V^{-1} s^{-1})
GaAs	5.4×10^5	—	2.7 (± 0.3)	1000 (± 100)	7000
InAs	3.0×10^3	5 (± 2)	1.4 (± 0.3)	6000 (± 1000)	22 700
InP	170	10 (± 3)	3.1 (± 0.5)	700 (± 100)	6000

given by

$$\omega_{0,N_p} = \sqrt{\frac{f N_p e^2}{m_e^* \epsilon_r \epsilon_0}}, \tag{3}$$

where ϵ_r is the static dielectric constant of the nanowires, ϵ_0 is the permittivity of free space and f is a constant dependent on the nanowire geometry and the surrounding dielectric medium [32, 34, 35]. For m_e^* and ϵ_r we use the values for bulk ZB semiconductors, namely $m_e^* = 0.063 m_e$ and $\epsilon_r = 12.95$ for GaAs nanowires, $m_e^* = 0.022 m_e$ and $\epsilon_r = 15.15$ for InAs nanowires and $m_e^* = 0.080 m_e$ and $\epsilon_r = 12.5$ for InP nanowires.

For doped samples and samples with small band gaps, there can be a significant carrier density present without photoexcitation. In this case, equation (2) is modified to

$$\Delta\sigma = \frac{i(N_p + N_{eq})e^2\omega}{m_e^*(\omega^2 - \omega_{0,N_p+N_{eq}}^2 + i\omega\gamma)}$$
$$- \frac{i N_{eq} e^2 \omega}{m_e^*(\omega^2 - \omega_{0,N_{eq}}^2 + i\omega\gamma)}, \tag{4}$$

where

$$\omega_{0,N_p+N_{eq}} = \sqrt{\frac{f(N_p + N_{eq})e^2}{m_e^* \epsilon_r \epsilon_0}}, \tag{5}$$

and

$$\omega_{0,N_{eq}} = \sqrt{\frac{f N_{eq} e^2}{m_e^* \epsilon_r \epsilon_0}}. \tag{6}$$

This modification accounts for the intrinsic and extrinsic carriers, with total equilibrium density N_{eq}, already present in the sample before photoexcitation. Equation (4) thus gives the change in conductivity under photoexcitation.

For each sample we performed a global fitting routine to its complete set of spectra, taken at various times after photoexcitation and at various fluences. We used N_{eq} and f as global fitting parameters, that is, fitting parameters held fixed for all spectra for a given sample. The photoexcited carrier density varies with fluence and with time after photoexcitation, so N_p was used as a local fitting parameter, that is, a parameter allowed to vary between spectra. Good fits were obtained for GaAs nanowires using the unmodified equation (2). This indicates that the ionized donor density, N_{eq}, in these nanowires was negligible. Accordingly, the fitted surface plasmon frequency, ω_0 follows equation (3). This is plotted in figure 3(d), which clearly shows ω_0 is proportional to $\sqrt{N_p}$ and passes through the origin when $N_p = 0$.

In the case of InAs nanowires, the fitting procedure gave an equilibrium carrier density of $N_{eq} = 6 \times 10^{15}$ cm^{-3}. As InAs is a narrow band gap semiconductor with a significant intrinsic carrier density, both intrinsic and extrinsic charge carriers contribute to N_{eq}. The intrinsic electron density in bulk InAs at room temperature is 7.8×10^{14} cm^{-3}. The remaining carrier density can be attributed to ionized donors, with a density of approximately $N_d = 5 \times 10^{15}$ cm^{-3}. This low level of unintentional doping is reasonable, firstly because surface states in InAs are donorlike and cause a surface electron accumulation layer which contributes to N_d [36, 37]. Secondly, carbon donors are likely to be present, because carbon is a decomposition product of trimethylindium during MOCVD growth [38]. Low growth temperatures, as employed for InAs nanowire growth, are known to increase the incorporation of carbon impurities as donors in InAs [38, 39]. Due to the intrinsic carrier density and background doping, the fitted surface plasmon frequency, ω_0, follows equation (5) as plotted in figure 4(d). When $N_p = 0$, ω_0 does not pass through the origin in figure 4(d), and instead intercepts at $\omega_{0,N_{eq}}$ as given by equation (6).

The terahertz conductivity response of InP nanowires has been analysed in detail in our previous publication [16], where we found it necessary to include background doping to fit to individual spectra. Here we improve upon the model presented in [16] by performing a global fit to all measured spectra, similar to the procedure described above for InAs nanowires. We deduce a background doping density of $N_{eq} = 1 \times 10^{16}$ cm^{-3}. The fitted surface plasmon frequency is plotted in figure 5(d).

The extracted scattering rates, γ, are summarized in table 1. Using these scattering rates we calculate the carrier mobilities via

$$\mu = \frac{e}{m_e^* \gamma}. \tag{7}$$

We calculate mobilities of 1000 cm^2 V^{-1} s^{-1} for GaAs nanowires, 6000 cm^2 V^{-1} s^{-1} for InAs nanowires and 700 cm^2 V^{-1} s^{-1} for InP nanowires. The mobility of InAs nanowires was the highest of all nanowires investigated, and is only a factor of 4 lower than typical electron mobilities in high quality bulk InAs at room temperature [40, 41]. This discrepancy between bulk and nanowire values may be due to higher surface scattering in InAs nanowires. Surface scattering can be marked in nanowires because of their large surface area-to-volume ratios. Surface scattering is anticipated to be particularly significant in InAs nanowires, because at InAs surfaces the Fermi level is pinned in the conduction band, producing an electron surface accumulation layer where

electrons experience increased surface scattering [37]. Surface passivation may be useful to unpin the Fermi level from the conduction band, and hence reduce surface scattering and produce higher electron mobilities approaching bulk values [42, 43]. Yet, even without surface treatment, the very high electron mobility measured highlights the potential of InAs nanowires for high mobility applications, such as in field effect transistors.

InP nanowires featured the lowest mobility. The mobility was significantly lower than values reported for optimized bulk InP [44], and we have previously shown that in these InP nanowires the mobility is limited by significant carrier scattering at ZB–WZ boundaries and stacking faults [16]. The GaAs and InAs nanowires investigated, on the other hand, are purely ZB, so their mobility values are not affected by scattering at ZB–WZ boundaries.

The mobility of GaAs nanowires was a factor of 6 lower than typical mobilities in bulk GaAs [45]. The lower mobility compared to bulk may be due to electron scattering at nanowire surfaces. In future, surface passivation, as used to improve carrier lifetimes, may improve the mobility in GaAs nanowires.

4. Conclusion

In summary, we have used OPTP spectroscopy to compare the electronic properties of GaAs, InAs and InP nanowires. We measured picosecond-long carrier lifetimes in GaAs nanowires, finding that the lifetime is severely limited by the extremely high surface recombination velocity. This indicates that highly effective surface passivation will be crucial for future GaAs nanowire-based devices. InP nanowires exhibited the longest carrier lifetimes and lowest surface recombination velocity, suggesting their potential for a number of optoelectronic devices including solar cells. InP nanowires, however, exhibited the lowest electron mobilities due to the high density of stacking faults and ZB–WZ polytypism. This presents a challenge to nanowire growers, to achieve phase-pure InP nanowires for higher electron mobilities. Finally, InAs nanowires exhibited very high electron mobilities of 6000 cm^2 V^{-1} s^{-1}, suggesting their immediate suitability for applications such as high electron mobility transistors.

Acknowledgments

References

[1] Czaban J A, Thompson D A and LaPierre R R 2009 GaAs core–shell nanowires for photovoltaic applications *Nano Lett.* **9** 148–54

[2] Wang J F, Gudiksen M S, Duan X F, Cui Y and Lieber C M 2001 Highly polarized photoluminescence and photodetection from single indium phosphide nanowires *Science* **293** 1455–7

[3] Duan X F, Huang Y, Cui Y, Wang J F and Lieber C M 2001 Indium phosphide nanowires as building blocks for nanoscale electronic and optoelectronic devices *Nature* **409** 66–9

[4] Tomioka K, Yoshimura M and Fukui T 2012 A III–V nanowire channel on silicon for high-performance vertical transistors *Nature* **488** 189–93

[5] Dayeh S A, Soci C, Yu P K L, Yu E T and Wang D L 2007 Influence of surface states on the extraction of transport parameters from InAs nanowire field effect transistors *Appl. Phys. Lett.* **90** 162112

[6] Wallentin J, Ek M, Wallenberg L R, Samuelson L and Borgström M T 2012 Electron trapping in InP nanowire FETs with stacking faults *Nano Lett.* **12** 151–5

[7] Titova L V *et al* 2007 Dynamics of strongly degenerate electron–hole plasmas and excitons in single InP nanowires *Nano Lett.* **7** 3383–7

[8] Hoang T B, Titova L V, Yarrison-Rice J M, Jackson H E, Govorov A O, Kim Y, Joyce H J, Tan H H, Jagadish C and Smith L M 2007 Resonant excitation and imaging of nonequilibrium exciton spins in single core–shell GaAs–AlGaAs nanowires *Nano Lett.* **7** 588–95

[9] Ketterer B, Uccelli E and Fontcuberta i Morral A 2012 Mobility and carrier density in p-type GaAs nanowires measured by transmission Raman spectroscopy *Nanoscale* **4** 1789–93

[10] Ulbricht R, Hendry E, Shan J, Heinz T F and Bonn M 2011 Carrier dynamics in semiconductors studied with time-resolved terahertz spectroscopy *Rev. Mod. Phys.* **83** 543–86

[11] Lloyd-Hughes J and Jeon T-I 2012 A review of the terahertz conductivity of bulk and nano-materials *J. Infrared Millim. Terahertz Waves* **33** 871

[12] Joyce H J *et al* 2011 III–V semiconductor nanowires for optoelectronic device applications *Prog. Quantum Electron.* **35** 23–75

[13] Dayeh S A, Aplin D P R, Zhou X T, Yu P K L, Yu E T and Wang D L 2007 High electron mobility InAs nanowire field-effect transistors *Small* **3** 326–32

[14] Joyce H J, Gao Q, Tan H H, Jagadish C, Kim Y, Zhang X, Guo Y N and Zou J 2007 Twin-free uniform epitaxial GaAs nanowires grown by a two-temperature process *Nano Lett.* **7** 921–6

[15] Joyce H J, Wong-Leung J, Gao Q, Tan H H and Jagadish C 2010 Phase perfection in zinc blende and wurtzite III–V nanowires using basic growth parameters *Nano Lett.* **10** 908–15

[16] Joyce H J *et al* 2012 Ultra-low surface recombination velocity in InP nanowires probed by terahertz spectroscopy *Nano Lett.* **12** 5325–30

[17] Parkinson P, Joyce H J, Gao Q, Tan H H, Zhang X, Zou J, Jagadish C, Herz L M and Johnston M B 2009 Carrier lifetime and mobility enhancement in nearly defect-free core–shell nanowires measured using time-resolved terahertz spectroscopy *Nano Lett.* **9** 3349–53

[18] Nolte D D 1990 Surface recombination, free-carrier saturation, and dangling bonds in InP and GaAs *Solid-State Electron.* **33** 295–8

[19] Léonard F, Talin A A, Swartzentruber B S and Picraux S T 2009 Diameter-dependent electronic transport properties of Au-catalyst/Ge-nanowire Schottky diodes *Phys. Rev. Lett.* **102** 106805

[20] Dmitruk N L, Lyashenko V I, Tereshenko A K and Spektor S A 1973 Investigation of surface recombination on epitaxial GaAs films *Phys. Status Solidi* a **20** 53–62

[21] Aspnes D E 1983 Recombination at semiconductor surfaces and interfaces *Surf. Sci.* **132** 406–21

[22] Mikhailova M P, Nasledov D N and Slobodchikov S V 1965 Spectral response of the photoeffects in InAs *Phys. Status Solidi* b **11** 529–34

[23] Casey H C and Buehler E 1977 Evidence for low surface recombination velocity on n-type InP *Appl. Phys. Lett.* **30** 247–9

[24] Diadiuk V, Groves S H, Armiento C A and Hurwitz C E 1983 Diffusion length of moles in n-InP *Appl. Phys. Lett.* **42** 892–4

[25] Rosenwaks Y, Shapira Y and Huppert D 1990 Metal reactivity effects on the surface recombination velocity at InP interfaces *Appl. Phys. Lett.* **57** 2552–4

[26] Chang C *et al* 2012 Electrical and optical characterization of surface passivation in GaAs nanowires *Nano Lett.* **12** 4484–9

[27] Sun M H, Joyce H J, Gao Q, Tan H H, Jagadish C and Ning C Z 2012 Removal of surface states and recovery of band-edge emission in InAs nanowires through surface passivation *Nano Lett.* **12** 3378–84

[28] Nienhuys H-K and Sundström V 2005 Influence of plasmons on terahertz conductivity measurements *Appl. Phys. Lett.* **87** 012101

[29] Berrier A, Ulbricht R, Bonn M and Rivas J G 2010 Ultrafast active control of localized surface plasmon resonances in silicon bowtie antennas *Opt. Express* **18** 23226–35

[30] Parkinson P, Lloyd-Hughes J, Gao Q, Tan H H, Jagadish C, Johnston M B and Herz L M 2007 Transient terahertz conductivity of GaAs nanowires *Nano Lett.* **7** 2162–5

[31] Parkinson P, Dodson C, Joyce H J, Bertness K A, Sanford N A, Herz L M and Johnston M B 2012 Noncontact measurement of charge carrier lifetime and mobility in GaN nanowires *Nano Lett.* **12** 4600–4

[32] Seletskiy D V, Hasselbeck M P, Cederberg J G, Katzenmeyer A, Toimil-Molares M E, Léonard F, Talin A A and Sheik-Bahae M 2011 Efficient terahertz emission from InAs nanowires *Phys. Rev.* B **84** 115421

[33] Strait J H, George P A, Levendorf M, Blood-Forsythe M, Rana F and Park J 2009 Measurements of the carrier dynamics and terahertz response of oriented germanium nanowires using optical-pump terahertz-probe spectroscopy *Nano Lett.* **9** 2967–72

[34] Pitarke J M, Silkin V M, Chulkov E V and Echenique P M 2007 Theory of surface plasmons and surface-plasmon polaritons *Rep. Prog. Phys.* **70** 1–87

[35] Chou L, Shin N, Sivaram S V and Filler M A 2012 Tunable mid-infrared localized surface plasmon resonances in silicon nanowires *J. Am. Chem. Soc.* **134** 16155–8

[36] Noguchi M, Hirakawa K and Ikoma T 1991 Intrinsic electron accumulation layers on reconstructed clean InAs(100) surfaces *Phys. Rev. Lett.* **66** 2243–6

[37] Dayeh S A, Yu E T and Wang D L 2009 Transport coefficients of InAs nanowires as a function of diameter *Small* **5** 77–81

[38] Fang Z M, Ma K Y, Cohen R M and Stringfellow G B 1991 Effect of growth temperature on photoluminescence of InAs grown by organometallic vapor phase epitaxy *Appl. Phys. Lett.* **59** 1446–8

[39] Thelander C, Dick K A, Borgström M T, Fröberg L E, Caroff P, Nilsson H A and Samuelson L 2010 The electrical and structural properties of n-type InAs nanowires grown from metal–organic precursors *Nanotechnology* **21** 205703

[40] Wieder H H 1974 Transport coefficients of InAs epilayers *Appl. Phys. Lett.* **25** 206–8

[41] Lloyd-Hughes J 2012 Generalized conductivity model for polar semiconductors at terahertz frequencies *Appl. Phys. Lett.* **100** 122103

[42] Jiang X C, Xiong Q H, Nam S, Qian F, Li Y and Lieber C M 2007 InAs/InP radial nanowire heterostructures as high electron mobility devices *Nano Lett.* **7** 3214–8

[43] van Tilburg J W W, Algra R E, Immink W G G, Verheijen M, Bakkers E P A M and Kouwenhoven L P 2010 Surface passivated InAs/InP core/shell nanowires *Semicond. Sci. Technol.* **25** 024011

[44] Razeghi M, Maurel P, Defour M, Omnes F, Neu G and Kozacki A 1988 Very high purity InP epilayer grown by metalorganic chemical vapor deposition *Appl. Phys. Lett.* **52** 117–9

[45] Beard M C, Turner G M and Schmuttenmaer C A 2000 Transient photoconductivity in GaAs as measured by time-resolved terahertz spectroscopy *Phys. Rev.* B **62** 15764–77